Int. J. Multiphase Flow Vol. 6, pp. 113–129

0301-9322/80/0401-0113/$02.00/0

CONDENSATION-DRIVEN FLUID MOTIONS

JAMES A. BLOCK
Creare Inc., Hanover, NH 03755, U.S.A.

Abstract—Direct contact condensation processes are examined to reveal common phenomena which govern fluid motions induced by condensation. A series of examples is presented and analysis assumptions and results are summarized and compared with data. A "universal" regime map for direct contact condensation is suggested. Although most examples discussed in this paper are taken from nuclear reactor safety researches, the methods presented are applicable to a variety of industrial and power generation processes.

1. INTRODUCTION

This paper describes phenomena, and provides numerous examples, where condensation processes influence, and are in turn influenced by, fluid motions. Areas are illustrated where a basic understanding of the interplay of condensation and fluid motions is important for assessing hardware, component, or system performance. This paper is not intended to be a literature review, and no universal formulation for dealing with problems of direct contact condensation is provided. However, common features of rapid condensation situations are illustrated, and this paper attempts to show where *ad hoc* analyses based on simplified physical processes have been successful. The methods summarized in this paper should prove useful for numerous applications including: nuclear reactor safety, boiler instabilities, waterhammer in two-phase systems, fossil, geothermal and solar power plants, chemical process industries, jet condensers, and spray cooling systems.

A common thread in many direct contact condensation situations is the usefulness of characterizing the system or process with a single dimensionless parameter which forms a scale for a rate, a transition in flow regime or a thermodynamic equilibrium. Examples of this will be illustrated. One useful condensation rate scale is obtained by examining whether heat transfer or other factors (such as liquid inertia) primarily govern the behavior. Specifically, when condensation is fast, gas dynamics often limit the phase transition rate and liquid inertia often dominates the fluid motion. When condensation is slower, the actual heat transfer rate must usually be determined as an integral part of the solution. Although in many situations the triggering of instability mechanisms determines whether condensation heat transfer is a controlling process, a parameter that has been used as a "scale" is the Jacob number: $\rho_L C_L(T_s - T_L)/\rho_G h_{LG}$. Subscripts L, G and S stand for liquid, vapor and saturation, respectively, throughout this paper. ρ is density, C is specific heat, h is latent heat and T is temperature. This expresses the ability of the liquid to absorb the energy released on condensation. An increased Jacob number favors large condensation rates and inertia-limited behavior. Examples will be presented to show the usefulness of this parameter and derivations from it.

Just as single-phase flows can be separated into categories of internal and external, direct contact condensation can be separated into problems where there is a complete vapor region collapse and where a distributed interface exists with no collapse. Although many similarities exist in the governing physical mechanisms at the interface, the fluid motion in situations without complete void region collapse are often related to system response in addition to the local condensation rate.

The collapse of small vapor bubbles has been a subject of intense interest in the field of

cavitation. Following the simple model of Rayleigh that predicted an infinite pressure at the time of collapse of a spherical bubble, attempts have been made to improve the analysis by considering effects of viscosity, nonspherical bubble shape, heat transfer, presence of gas in the bubble, proximity of boundaries, and liquid compressibility. Hickling & Plesset (1964) obtained impact pressures of the proper order of magnitude, Florschuetz & Chao (1965) predicted bubble collapse rates that compared favorably with measurements, and Biasi *et al.* (1972) showed that the pressure pulses are reduced by including liquid compressibility in the analysis. Board & Kimpton (1974) investigated bubble collapse for the range of subcooling for which full coupling of inertia and heat transfer occurs and they measured bubble collapse rates which compared reasonably well with theory for subcoolings up to 60°C. A summary of the available theories of nonequilibrium bubble collapse is provided by Theofanous *et al.* (1969). However, these investigations concentrated on small bubbles (generally in the less than 10 mm range), while this paper discusses the collapse of large voids (up to the order of 1 m or more in extent).

The collapse of voids in ducts has been studied as part of the "column separation" problem. Most authors report that results can be predicted by ignoring heat conduction and assuming that the steam is always at the equilibrium vapor pressure. Attempts to model thermal effects using transient conduction theory, as done by Lee (1962) and Hawtin *et al.* (1970), may not be appropriate near a turbulent or nonplanar interface usually associated with very large voids. Kosky & Henwood (1969) collapsed vapor cavities in the frustrum of a cone and generated peak pressures up to 130 MPa. Using the same apparatus, Hawtin *et al.* (1970) found that heat transfer effects were important for water subcooling below 45°C, but for subcoolings above 45°C inertia effects were dominant. Many of these methods and results are useful in the understanding of steam void collapse in reactor safety applications.

Workers concerned with condensation without void collapse have tended to focus on the condensation rate. Bankoff *et al.* (1978), who suggest a strong coupling between liquid phase turbulence and condensation, attempted to deduce the local condensation rate in concurrent horizontal stratified flow of steam and subcooled water by measuring the total steam flux at various axial positions. This technique however is not capable of resolving details very near the initial contact region, as would be important for example, in core spray behavior. Attempts to determine condensation rates by the effect of condensation on the fluid dynamics [as done in ECC bypass studies, see for example Block & Schrock (1977)] have similarly not dealt with local mechanisms. Maa (1969) performed experiments where he briefly exposed a highly subcooled liquid jet and found that the condensation rate appeared to be limited only by sonic velocity in the vapor phase. Although it is not the intent of this paper to deal with kinetic theory aspects of condensation, it is observed here and shown later by example that under some conditions condensation limited by a local or upstream Mach number of order unity can be a very useful assumption.

A number of specific examples of condensation-induced fluid motions are discussed in this paper and high-speed movies of several of these examples have been made. These examples deal both with situations where condensation drives liquid motion by creating a local region of reduced pressure and where the condensation-induced vapor flows can themselves drive liquid motion.

2. BISTABLE EFFECTS

Rothe & Block (1977) have analytically treated the effect of entrained (noncondensible) gas flows on the trajectories of droplets in a liquid spray. They showed that the gas entrained into the spray by the axial motion of the liquid drags the drops radially inward and thus contracts the spray—an effect that becomes more pronounced as the pressure (gas density) is increased. In a situation such as a BWR core spray system, this effect can be augmented by steam flow induced into the spray by condensation on subcooled drops as illustrated in figure 1 which shows a typical pressure-atomizing liquid spray nozzle. At very high subcoolings, the rate of

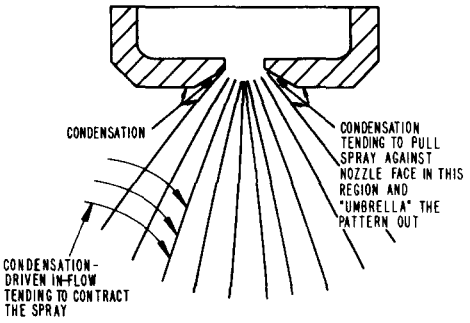

Figure 1. Mechanisms for pattern broadening or contraction of a liquid spray.

condensation on the issuing jet is very rapid just as it leaves the nozzle. There is also condensation on the surface of the nozzle. This leads to a depression of pressure in the region close to the nozzle exit and a tendency to prevent separation of the jet from the nozzle. The water then tends to flow along the bottom face of the nozzle and produce an "umbrella" pattern. As conditions (principally subcooling and nozzle-to-environment pressure difference) vary, the spray pattern can jump from the normal narrow cone to the broad umbrella distribution and back again. A modification of the nozzle exit geometry to preclude this bistable effect successfully eliminated the undesirable umbrella pattern.

3. INDUCED MOTIONS IN COUNTERCURRENT FLOWS

Countercurrent flow situations are important to safety analyses in a number of reactor components: PWR downcomer annulus during ECC injection, the upper plenum and core region of a PWR or BWR during a postulated LOCA, the feedring holes of PWR steam generators after a loss of level, etc. Two examples are given here for condensation-driven fluid motions from studies of ECC bypass in model PWR downcomers, a situation reviewed by Block & Schrock (1977). Referring to figure 2, the main parameter of interest in these studies is the timing and rate of ECC liquid delivery to the lower plenum against the upward flow of steam which tends to force the liquid out the broken cold leg. Since the fluid behavior in the downcomer region is influenced by the system response—particularly the supply characteristics of the steam source—we first digress to define steam supply characteristics. These definitions will be useful throughout this paper.

In general, we speak of "hard" steam supplies when the resistance is high and capacitance is low between the steam supply and the region of interest. In this case the steam flow rate is relatively independent of the condensation process. Conversely, we speak of a "soft" steam supply when the resistance is low between the steam supply and the condensation region and

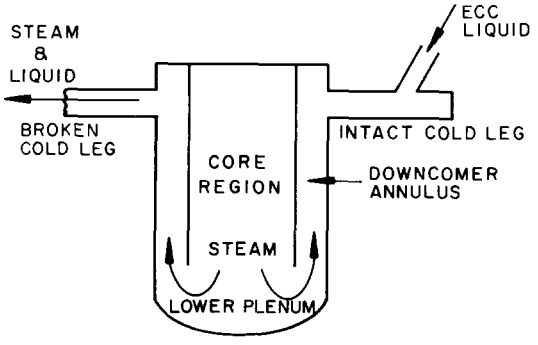

Figure 2. Schematic of flows during a postulated LOCA in a PWR.

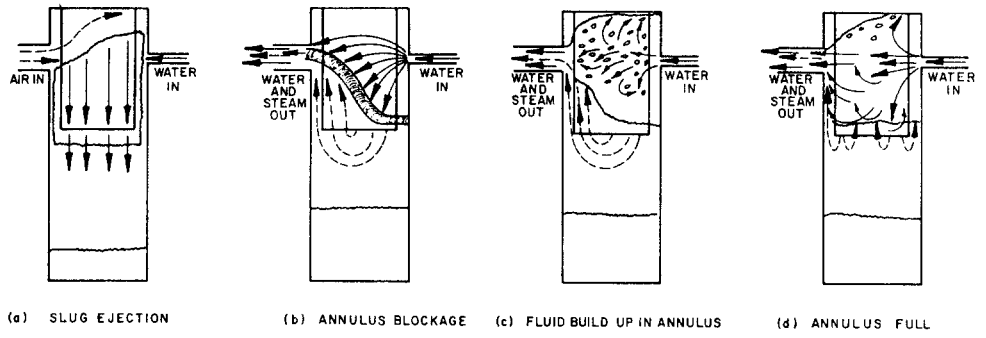

Figure 3. Artist's conception of the sequence of slug delivery (from high-speed movie).

the steam flow rate is very responsive to pressure changes caused by condensation and other factors. Specifically for ECC bypass, in experiments with a hard steam supply, the water delivery in the lower plenum tends to be oscillatory with periods of rapid liquid flow to the lower plenum ("slug delivery") and periods of no liquid delivery at all to the lower plenum. When the steam supply is soft, slug delivery tends not to occur but condensation on the subcooled ECC liquid can induce additional steam flow up the annulus. During a LOCA a PWR would more closely resemble the soft steam supply case since the reactor steam comes from flashing and heat transfer in the core and lower plenum as well as other regions.

3.1 *Annulus flow oscillations*

Here we consider the situation reported by Block & Crowley (1976) where the steam supply is hard (its flow rate is fixed by a choked valve) and the ECC liquid, also flowing at an experimentally-fixed rate, is higly subcooled. One cycle of slug-delivery oscillation is sketched in figure 3, the lower plenum pressure measured in a 1/30-scale glass model is shown in figure 4, and the measured transient annulus liquid fraction and lower plenum water volume from a 1/15-scale experiment are shown in figure 5. Three characteristic time periods can be seen in the pressure trace of figure 4. Since virtually all of the liquid stored in the annulus (together with the liquid entering from the cold leg) enters the lower plenum during the slug delivery period (A) as can be seen from figure 5, and since periods A and B are normally much shorter than period C, the time-averaged flow rate of liquid to the lower plenum can be reasonably well predicted by analyzing the liquid storage and duration of the waiting period (C). Experimentally period C varies from 0.5 to 20 s as (principally) the steam and liquid flow rates are changed.

The waiting time is postulated to be due to relaxation processes occurring in annulus. After a slug delivery, the annulus is virtually empty of water. An equilibrium situation is then approached as part of the injected water accumulates in the annulus and provides increasing surface area and heat capacity for condensation thus reducing the effective steam flow out of the annulus. Eventually the net (injected minus condensed) annulus steam flow falls below a

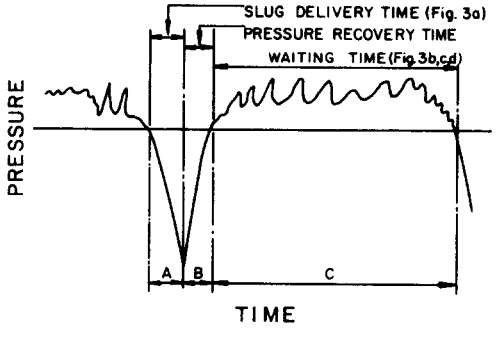

Figure 4. The major features of a typical lower plenum pressure trace with slug delivery.

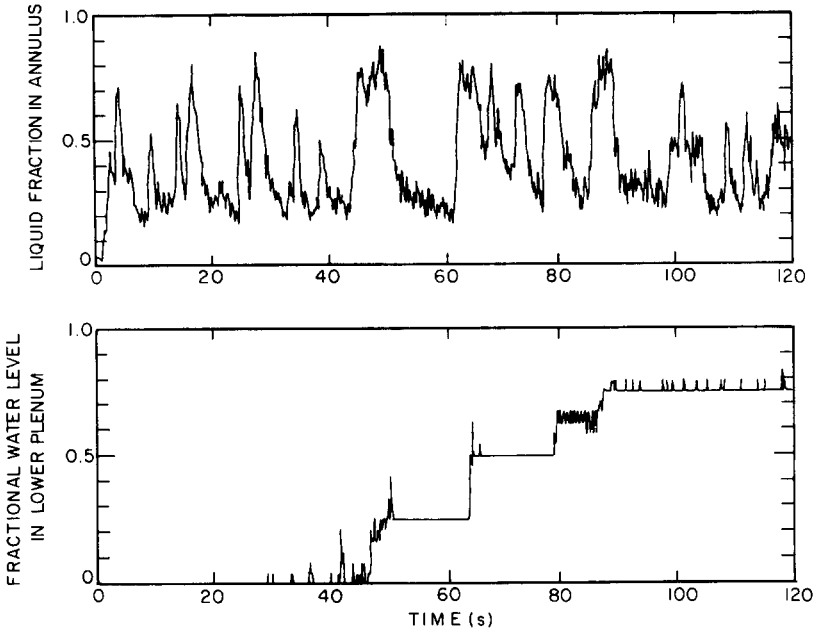

Figure 5. Annulus liquid fraction and lower plenum water level during a test with slug delivery.

critical level, as reported by Block *et al.* (1976) and Rothe & Crowley (1978), which allows some penetration of water into the lower plenum. This greatly increases the exposed surface area of subcooled water, causes rapid steam condensation, and drops the pressure in the lower plenum. The pressure difference between the upper annulus and the lower plenum then acts to drive the contents of the annulus downwards. This causes further condensation and the process is self-reinforcing, culminating in the delivery of the entire contents of the annulus. Violent agitation observed on the surface of the water falling into the lower plenum during this process is evidence of this rapid condensation.

An analysis has been written in Rothe *et al.* (1978b) using this model of the coupled thermal and momentum exchange processes in the downcomer. This analysis is shown compared with a typical body of data in figure 6. The analysis also predicts the period of the slug delivery oscillations, as indicated by the numbers near the curves, and these compare favorably with the data. A detailed prediction of the pressure variations and of time periods A and B in the pressure trace of figure 4 remains to be developed.

A regime map for slug delivery behavior is presented in figure 7. A necessary, but not sufficient, condition for slug delivery is that the thermodynamic ratio $R_T = C_L(T_s - T_L)\,W_L/h_{LG}W_G$ is greater than unity, where W is mass flow rate. This parameter, which is related to the Jacob number, expresses the capability of the liquid to absorb the latent heat of the steam that is flowing. It will be shown useful for characterizing transitional behavior in other examples which follow.

At low liquid enthalpy flow rates, hydrodynamic effects dominate downcomer flooding behavior as well as the flooding behavior discussed in section 3.3.

3.2 *Condensation-induced transients*

In the opposite situation of a very soft steam supply, the steam flow rate is not fixed but can respond to the reduced pressure caused by condensation in the annulus and broken cold leg. The increased steam flow rate thus induced can bypass the liquid out the break. This behavior has been observed experimentally in 1/15-scale tests of Crowley *et al.* (1977) and in tests in the Semiscale system.

A particularly revealing example of this behavior is Semiscale S-01-1B reported by Crapo *et*

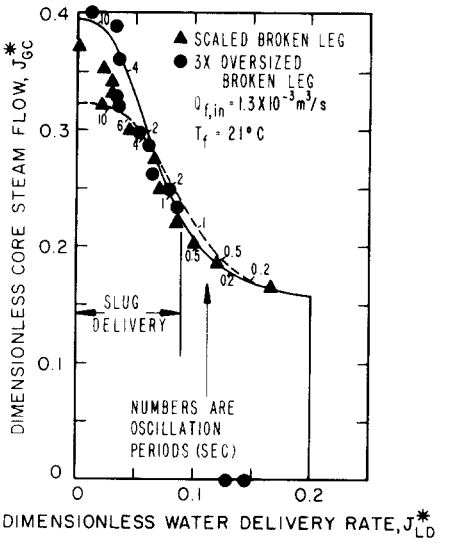

Figure 6.

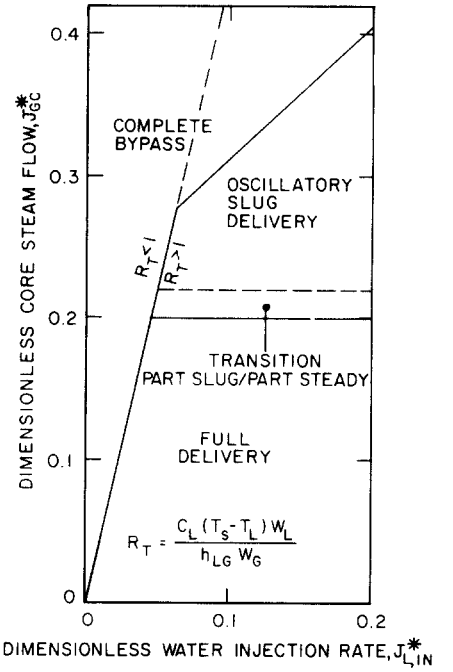

Figure 7.

Figure 6. Comparison between slug delivery theory and experiment.
Figure 7. Annulus delivery regime map with 21°C water.

al. (1975), which was a *hot-leg* break test. Prior to subcooled ECC injection into the cold legs, the steam velocity in the annulus was downward; at ECC injection the annulus steam flow direction changed to upward, remained significantly upward for about 40 s, and essentially prevented delivery of the ECC injected during this period. Analysis of this test [see Appendix A of Crowley *et al.* (1977)] reveals that the primary source of the steam upflow during this period was the flashing and boiling of the lower plenum liquid which was not swept out during the blowdown. In many Semiscale tests bypass continued until either the flashable liquid supply was exhausted, or until the accumulator liquid supply was exhausted. When the flow of subcooled ECC is stopped, the liquid stored in the annulus and cold leg is heated to saturation by the steam. This then stops the condensation-induced steam flow and permits the stored liquid to fall to the lower plenum.

It has also been shown experimentally by Crowley *et al.* (1977) that condensation on the injected subcooled liquid will increase the steam flow such that there is a "universal" flooding curve that is remarkably insensitive to steam supply compliance. Thus, the analysis of system behavior in a compliant system like a PWR must focus on those factors that determine the steam flow rate: the flashing and boiling capability of the regions containing saturated liquid, the break pressure drop with two-phase flow, and the rate of condensation in the downcomer and cold legs.

3.3 *Flooding at perforated plates*

A situation occurring in the chemical process industry and in flooding from above nuclear reactor cores consists of liquid downflow through a perforated-plate-like geometry against a vapor upflow. When the injected liquid is subcooled the $R_T = 1$ condition forms an approximate boundary separating regions of no liquid downflow and some liquid downflow and a regime map very similar to that of figure 7 is appropriate. When the steam is superheated, its sensible heat must be added to the latent heat term in the denominator of R_T as illustrated by the data of Bankoff (1979) shown in figure 8.

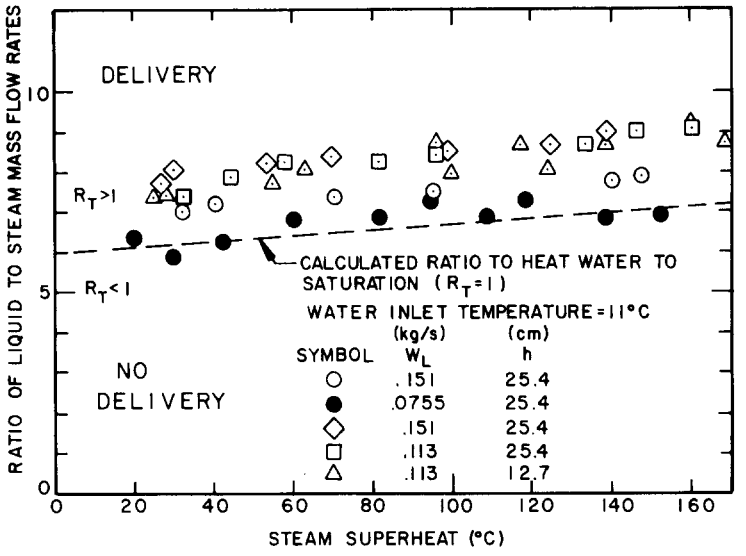

Figure 8. Onset of delivery ("weeping") data from top flood experiment of Bankoff (1979).

4. RAPID CONDENSATION-INDUCED MOTIONS—VERTICAL

Examples of large vapor region collapse upon triggering of rapid condensation are discussed in this section.

The simplest geometry to consider is a vertical pipe with its exit submerged in a large pool of subcooled water and with steam flowing into the top of the pipe. A range of behaviors is possible as the steam flux and pool subcooling are varied. The flow regime map from Chan *et al.* (1978) shown in figure 9 forms a useful basis for discussion.

At very high steam flux, the steam will bubble through the pool, much as a noncondensible gas would, if the pool subcooling is low, while with high subcooling a noisy condensation "flame" will exist at the pipe exit as studied extensively by Stanford & Webster (1972). At very low steam flux a stable, quiescent interface will exist near the pipe exit as the condensation rate is continuously equal to the steam supply rate. This flat interface produces the low rate end of a condensation rate scale; the latent heat released by condensation is simply removed by conduction in the liquid (neglecting natural convection in the pool). At the other extreme, mixing in the pool and creation of additional interface can lead to such potentially high rates of condensation that the actual rate of condensation is limited by the rate at which the system can supply steam to the interface. This "gas dynamic" limit is reached when the Mach number of

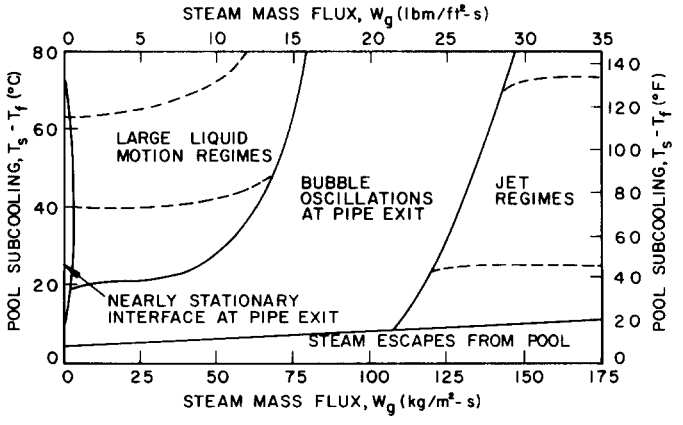

Figure 9. Approximate regime map for steam injection into a pool by Chan *et al.* (1978).

the steam flow reaches unity at the "governing cross-section area", as suggested by Maa (1969). It is argued here that there is often a sudden transition to this high rate regime as both the induced water motion refreshing the interface with subcooled water and the steam shattering of the interface promote condensation. This case of intermediate steam flux and high pool subcooling is often of greatest practical interest and is treated in this section where it is shown that the instantaneous condensation rate rarely equals the time-averaged steam supply rate. This imbalance leads to pressure transients which give rise to gross liquid movements.

4.1 *Hard steam supply*

Rothe *et al.* (1977a, 1978a) describe an experiment where steam was introduced at a constant (choked) rate though a small tube penetrating the top cap of a larger 0.7 m long vertical tube whose end was submerged in a very large pool of subcooled water. The steam would gradually warm the water in the tube and void the tube of water. Sometime after the steam-water interface reached the bottom of the tube, sudden exposure of steam to cold water there initiated rapid condensation and a collapse of the void. The water column rose rapidly in the tube, reaching the capped end in about 100 ms. There was a loud noise, visible shaking of the pipe, and a 1 ms duration overpressure pulse of about 7 MPa in atmospheric pressure experiments and about 14 MPa in experiments performed at 5 atm pressure.

A simple analysis of this process neglects gravity and friction, assumes rapid condensation is suddenly triggered (perhaps by interface shattering), and assumes that the pressure in the tube is constant as the slug forms and moves. It can then readily be shown that the liquid slug moves up the tube at a constant velocity given by $V = \sqrt{(\Delta p/\rho_L)}$ where Δp is the pressure difference acting on the slug. From waterhammer theory the overpressure on impact is $\rho_L a V$, where a is the sound speed in water, and the duration of the overpressure pulse is $2L_s/a$, wher L_s is the slug length.

Figure 10 gives sample pressure traces from atmospheric pressure tests. An underpressure of $3\text{–}5 \times 10^{-2}$ MPa implies a slug velocity of about 5–6 m/s. A 7 MPa overpressure implies a slug velocity of about 5 m/s. And the duration of the overpressure pulse is consistent with a slug which is the same length as the tube.

A more completed analysis by Rothe *et al.* (1977a), which does not assume constant pressure in the void, addresses the question of whether this behavior is limited by the condensation rate or by liquid inertia. The equation

$$\frac{\mathrm{d}}{\mathrm{d}t^*}\left[x^*\frac{\mathrm{d}x^*}{\mathrm{d}t^*}\right] = \frac{C^*t^* - x^*}{1 - x^*}$$

results where x^* and t^* are dimensionless slug position and time. The dimensionless condensation coefficient C^* is essentially the ratio of the condensation velocity (the condensation rate divided by $\rho_G A$ where A is the area) to the slug velocity given by $(\Delta p/\rho_L)^{1/2}$. If C^* is greater than about 0.34, the condensation proceeds rapidly enough to drop the pressure to near zero and the slug motion tends to be inertia limited. (In this case the expected over pressure would be about twice that observed in these tests.) A very low value of C^* implies the process is limited by condensation heat transfer and the slug moves only as fast as the volumetric removal of steam from the void. Figure 11 shows these limits and the transition predicted by this analysis, and figure 12 shows calculated pressure transients in the void as C^* is varied. The end of each curve on figure 12 corresponds to the impact of the slug on the end of the pipe.

4.2 *Softer steam system*

A softer situation is achieved by adding a volume between the steam supply and the tube (which is now fully open on both ends). In this case the capacitance of the volume is important since additional steam can be supplied to the condensing region as in the example of

condensation-induced transients. (Completing the admittedly imperfect analogy, the slug motion just discussed parallels the hard steam supply situation that led to downcomer oscillations.) Experiments have been performed at Creare where the previously-described vertical tube experiments was modified by adding a volume upstream of the tube and replacing the very large pool by a 152-mm-dia. glass vessel to permit easy flow visualization and high speed movies.

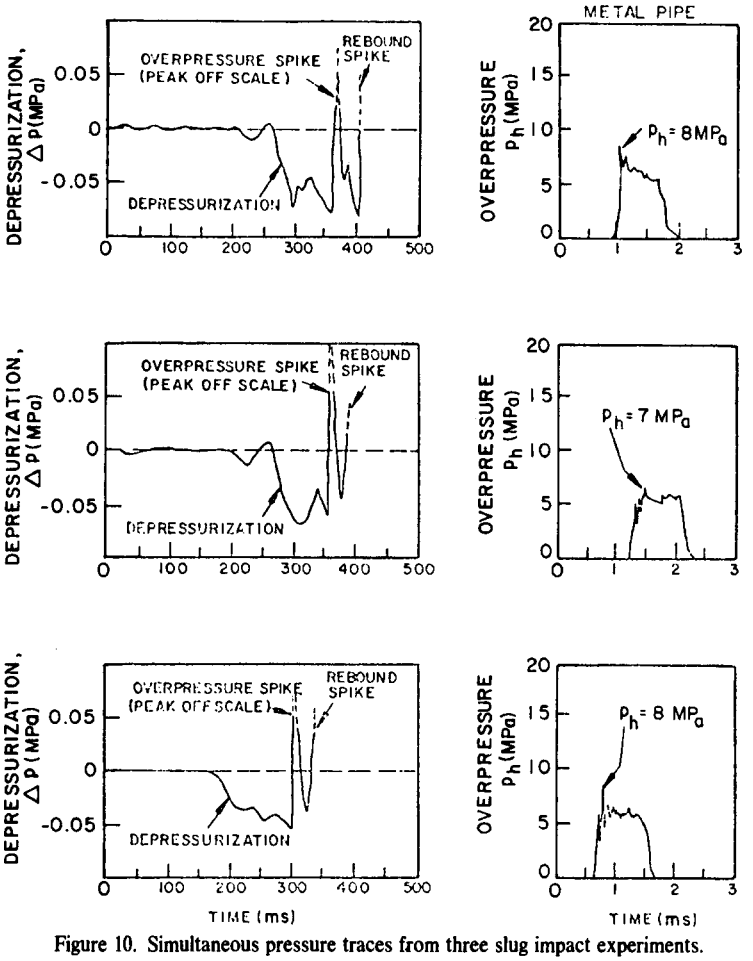

Figure 10. Simultaneous pressure traces from three slug impact experiments.

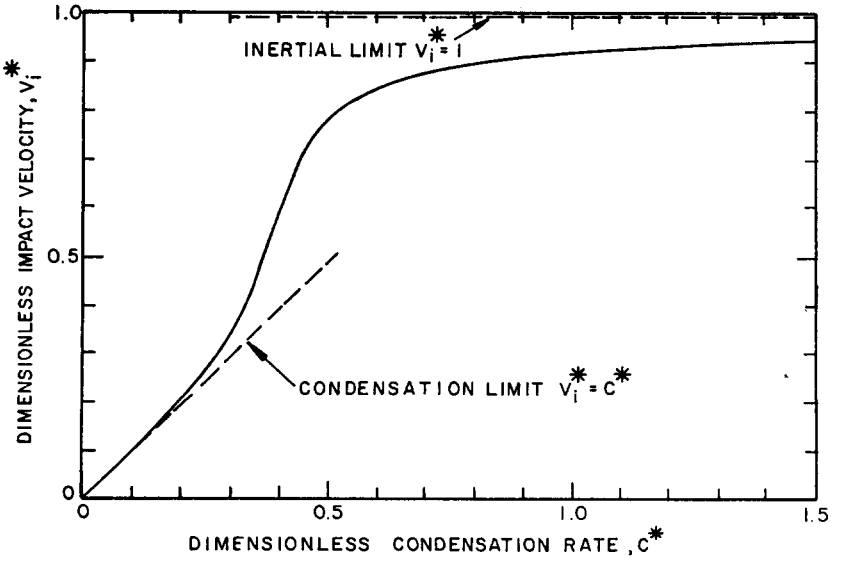

Figure 11. Impact velocity vs condensation rate on dimensionless coordinates.

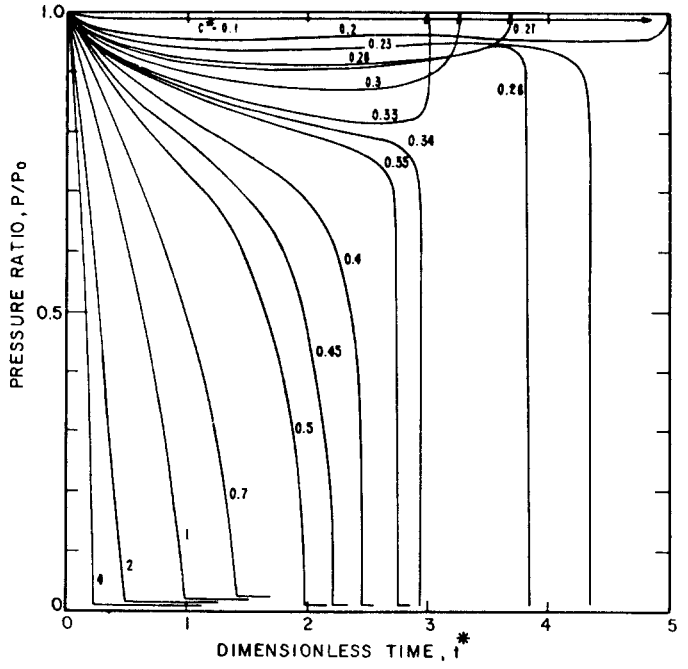

Figure 12. Dimensionless pressure history in the void for various condensation rates, C^*.

Figure 13 shows the pressure measured in the tube and liquid for one selected condensation event. Just as described above, water is expelled from the tube by the steam inflow. A bubble forms at the mouth of the tube and grows. During the growth the condensation rate is relatively low as indicated both by the shiney and relatively smooth, though lobed, bubble surface (see figure 14a) and by instruments in the tube and upstream volume. At about the time the bubble reaches its maximum size a dark haze on the bubble surface appears (figure 14b). This is believed to be due to the onset of an interfacial instability that triggers extremely rapid condensation by interface shattering. This is confirmed by a rapid decrease of pressure in the tube and the liquid. The dark haze grows (figure 14c) and the pressure levels off.

From about this point until somewhat after the bubble has collapsed, analysis of instruments in the tube and upstream volume show that a nearly steady steam flow has been established corresponding to a Mach number of about unity in the tube. This implies that condensation is proceeding so rapidly that the rate of vapor removal is not limited by heat transfer but by the rate at which vapor can be supplied to the interface. Convection (induced motion and turbulence) mechanisms in the liquid might account for this high condensation rate, or it could be explained by interface shattering exposing very large amounts of subcooled liquid.

As the bubble begins to collapse, the pressure in the bubble rises somewhat but then falls

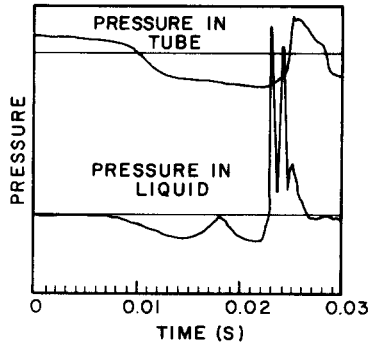

Figure 13. Pressure traces for one condensation event.

again as the bubble begins to detach from the vent restricting the flow of steam to the bubble (figure 14d). This changing pressure is seen in the liquid but not in the tube because the flow in the tube is choked. At 0.023 s a sharp spike occurs in the pool pressure trace. This is almost exactly the time at which complete bubble collapse is seen to occur on the film. The liquid then flows into the tube driven by the reduced pressure there and in the upstream volume. However, unless the tube is very short or the steam flow rate very low, the greatly reduced condensation rate on the interface moving up the tube causes the slug to decelerate and reverse in the tube and the cycle repeats. It should be realized that each such condensation event is different in detail and a particularly clean event was chosen for this example.

In this particular situation with high liquid subcooling the condensation rate is either very low or very high. When it is high, the details of the condensation process are relatively unimportant, since the rate is gas dynamics limited, and an analysis of the gross liquid motion is rather straightforward. This has been done by formulating mass and momentum balances for the several regions of importance and assuming a simple on–off model for the condensation driver. This analysis, which has been shown to be valid over a range of conditions, is assisted by the empirical observation that the condensation time period is relatively insensitive to a variety of fluid, thermal, and geometric parameters. Thus the event frequency is simply proportional to the ratio of the time-averaged steam flux to the instantaneous maximum possible steam flux. Other analysis by Sargis *et al.* (1978), Sursock & Duffey (1978) and Brennen

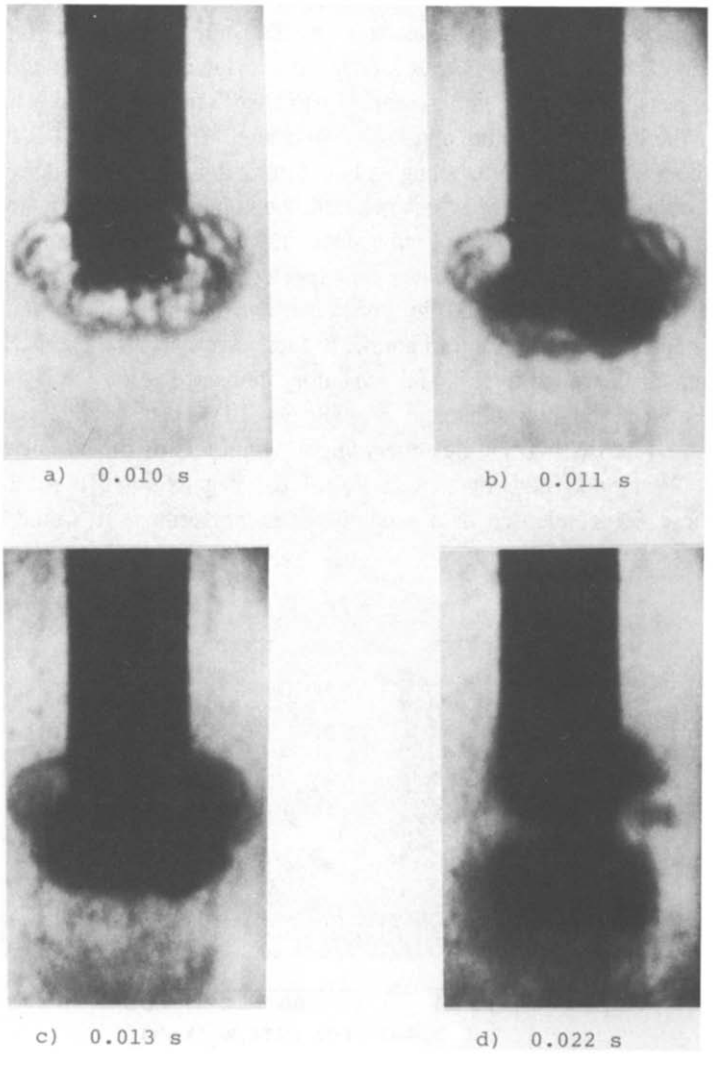

Figure 14. Frames from movie for the condensation event of figure 13.

(1978) of similar situations have not contained these features but have explored other aspects of this phenomenon.

5. RAPID CONDENSATION-INDUCED MOTIONS—HORIZONTAL

This section provides three examples of rapid condensation inducing pressure and flow excursions in horizontal pipes. Many of the same ideas that proved useful in understanding the behavior in the previous examples will be seen to also be useful for these.

5.1 *Jet condensers*

Westendorf & Brown (1966) have studied the condensation of steam injected inside a concurrent subcooled water steam flowing horizontally through a 25-mm-dia. tube at atmospheric pressure. They found three modes of instability: (i) random high-frequency pressure fluctuations; (ii) regular low-frequency oscillations; and (iii) interface excursions. As observed in other condensation situations, the amplitudes of the fluctuations were directly proportional to the coolant inlet subcooling and flow rate. Their major findings are summarized in figure 15.

Westendorf & Brown (1966) compared their findings to boiler stability data and subcooled boiling instabilities. However, the phenomena discussed in the preceding sections provide explanations for the regimes of figure 15. As stated at the beginning of section 4, when the subcooling is high, a noisy condensation "flame" will exist where the condensation rate is high and remains high enough (because of the sustained shattering of the interface by the steam flux) to continuously condense the supplied steam. Thus, the flame-like interface remains in roughly the same location though it moves about locally rather violently. When liquid is also flowing, this behavior is possible when the liquid's capacity to absorb the latent heat is high, that is when the *product* of the liquid subcooling and flow rate is high. Thus, Region I is expected to exist above a hyperbola on a plot of subcooling vs liquid mass flow rate—as it does on figure 15.

As the subcooling or liquid flow rate is reduced, the condensation rate is lowered and it can no longer keep up with the steam supply in a steady manner. Thus, oscillations associated with highly variable (in time) condensation rates are expected and observed. Finally, the liquid is no longer able to condense the supplied flow of steam and an interface excursion occurs. This parallels the complete bypass region of figure 7. In fact, exactly the same criterion ($R_T = 1$) that formed the boundary between bypass and oscillatory delivery for the PWR downcomer forms the boundary between the interface excursions (Region III) and the oscillations (Region II) for the jet condenser—the $R_T = 1$ line lies everywhere within 6°C of the regime boundary drawn empirically by Westendorf & Brown, with $R_T < 1$ forming Region III. Although a complete analysis of these jet condenser data has not been performed, it would be a relatively

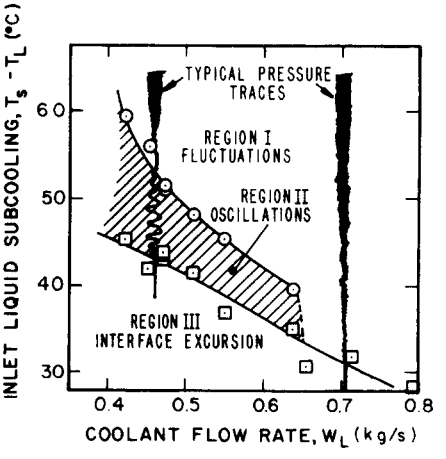

Figure 15. Instability regions for jet condenser at $W_G = 0.034$ kg/s from Westendorf & Brown (1966).

straightforward job using these observations and the formulation referenced in the next subsection.

5.2 *Cold leg flow oscillations*

The cold leg of a PWR during a postulated LOCA is essentially a horizontal pipe with steam flow and with subcooled ECC liquid injected into it through a smaller diameter pipe as illustrated in figure 16. Under certain conditions (described below) a water plug will move in an oscillatory manner in the pipe at frequencies from about 0.1 to 10 Hz with the following characteristics. With a liquid plug downstream of the injection location (see figure 16), steam can condense rapidly on the exposed cold jet and the upstream-facing surface of the plug (at position x). This reduces the pressure in Region I, slowing and reversing the interface velocity. When the interface moves upstream of the injection location, the cold ECC jet is covered and the interface warms rapidly to the saturation temperature. Condensation ceases and the pressure in Region I builds up and over-shoots slowing, stopping, and reversing the upstream motion of the plug. Moving downstream again, the plug interface uncovers the cold water jet as it passes the injection point and rapid condensation is possible again. The cycle is repeated periodically.

A dynamic analysis has been developed in Rothe *et al.* (1977b) to model this behavior. An "on–off" model of condensation is employed with the condensation rate at the limit necessary to achieve thermodynamic equilibrium ($R_T = 1$) when the plug is downstream of the injection leg and no condensation at all when the plug is upstream of the injection leg. One-dimensional flow models of conservation of mass, momentum and energy are employed and the resultant analysis accurately predicts the complicated lines between the three primary regimes of behavior shown on figure 17. The analysis also successfully predicts wave shapes and amplitudes of the pressure oscillations and oscillatory frequencies measured by a variety of researchers at a range of scales from 1/20 to 1/3 of PWR scale. This analysis has been used to predict behaviors in Semiscale, LOFT and PWRs by Rothe *et al.* (1976). A recent LOFT test (L2-2) reported by Batt (1978) had such cold leg oscillations beginning just after ECC injection and lasting for about 30 s.

As in other examples discussed in this paper, the analysis is facilitated by the fact that an on–off model for condensation is a good approximation to reality. When condensation is "on", it is so rapid that the rate is controlled by gas dynamics and the liquid motion is inertially limited. Again the $R_T = 1$ condition provides a good indication of a major regime boundary

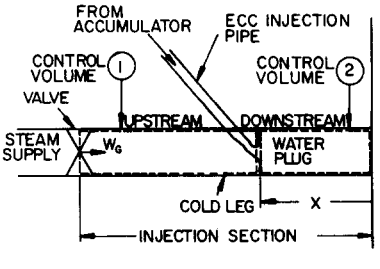

Figure 16. Model for analysis of cold leg oscillations.

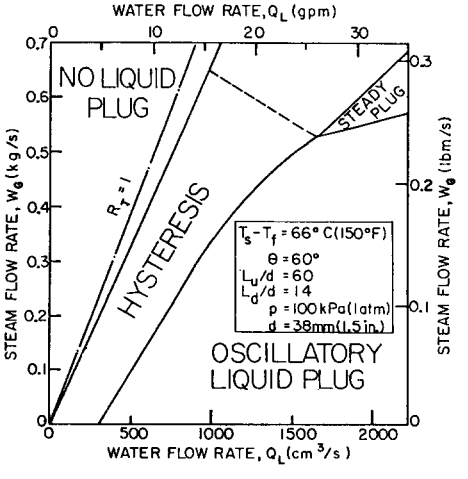

Figure 17. Cold leg flow regime map.

(figure 17) and, as seen for jet condensers and the downcomer annulus, the region $R_T < 1$ is characterized by a downstream excursion of the liquid while the region $R_T > 1$ has either oscillations or steady condensation of all the steam flow (but sometimes with noisy, high frequency fluctuations).

5.3 *Condensation-induced waterhammer*

When subcooled liquid flows through a partially filled horizontal pipe into a steam filled region, the countercurrent flow of steam induced by condensation can cause waves on the liquid surface which can block the pipe with a liquid plug. When this happens, a steam void is trapped and, if conditions are right, rapid condensation can be triggered in the void. This can then accelerate the slug (as in the vertical tube previously discussed) and slug impaction on pipe bends or area changes can induce substantial waterhammer loads.

This process has been studied at small scale (38-mm-dia. pipe) by Rothe *et al.* (1977a, 1978a) who observed overpressure spikes up to 5 MPa in experiments at one atmosphere and 10 MPa at 5 atm. When 0.05 and 0.13% air (by mass) was added to the steam, the overpressures were reduced by factors of 2 and 20, respectively, at atmospheric pressure. This exemplifies the powerful effect air has on all rapid condensation processes. By examing the characteristics of the underpressure traces measured at this scale without air, it can be concluded that, although condensation could be very rapid once a vapor region was formed, it often was quite slow and only occasionally approached a purely inertia-limited behavior ($C^* \geq 0.5$). However, there is evidence that a very high C^* has occurred in a reactor waterhammer as discussed below.

Of the significant waterhammer events that have occurred in reactor systems, one [at Tihange reported by Batchelor (1976)] resulted in the high-response rate pressure record shown in figure 18. The pressure in the pipe decreased from 7 MPa to near zero in about 20 ms and remained low for about 35 ms while a slug was accelerated in the pipe. The resultant overpressure was 41 MPa. If condensation is assumed to have proceeded at a steady, equilibrium rate dictated only by the water injection rate and $R_T = 1$, then this would imply $C^* \simeq 0.05$. Clearly rapid void collapse cannot occur at such a low C^*. However, since it did occur at Tihange, condensation must have been strongly enhanced by sudden exposure of the pool of cold water stored in the pipe. The Tihange data show a ratio of dwell time at low pressure to depressurization time of about 1.7 which corresponds to a value of C^* of about 2 in figure 12. Furthermore, if one assumes an initial void size consistent with the geometry and a condensation rate limited only by gas dynamics (i.e. Mach 1 at one end of the void), the calculated depressurization time is consistent with the observed time. As characterized by C^*, this event was closer to being purely inertially limited than any other condensation event known to this author.

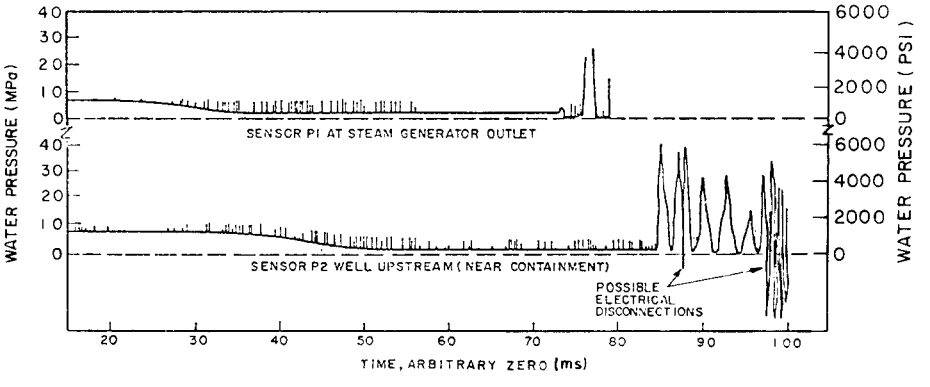

Figure 18. Pressure histories in feedwater pipe at Tihange from Batchelor (1976).

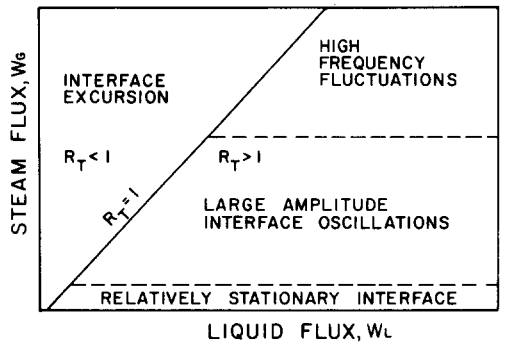

Figure 19. "Universal" regime map for direct contact condensation.

6. CONCLUSION

Perhaps the most useful way to summarize and conclude is to suggest an approximate "universal" flow regime map for direct contact condensation. Figure 19 shows this map. The $R_T = 1$ line separates the map into two major regions where complete condensation of the steam is not possible ($R_T < 1$) and where it is possible ($R_T > 1$). The $R_T > 1$ region is subdivided by dashed lines which may curve upward or downward. This map is actually a plane normal to the third axis, the liquid subcooling. As the subcooling is increased, the $R_T = 1$ line (surface) rotates toward the W_G-axis and the dashed lines (surfaces) move away from the W_L-axis as illustrated schematically in figure 20.

This map can be compared with the hard steam supply examples in figures 7, 8, 15 and 17 for the downcomer, "perforated plate", jet condenser and cold leg, respectively. In downcomer experiments at high steam flow, the amplitude of pressure fluctuations in the complete bypass region increases as the liquid flow rate is increased, consistent with figures 19 and 20. Additionally, as the subcooling is increased, the oscillatory region grows in size, and at low steam flows the complete delivery region is characterized by complete condensation on a relatively smooth and stationary interface. This map is also consistent with figures 15 and 17 (the steady plug region of figure 17 was indeed characterized by high frequency fluctuations), though neither

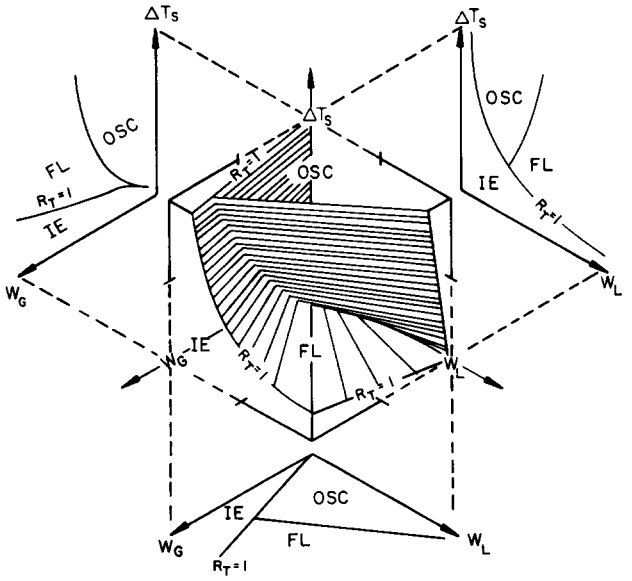

Figure 20. "Universal" three dimensional regime map for direct contact condensation with projections onto the three planes. (IE = Interface Excursions; FL = High Frequency Fluctuations; OSC = Large Amplitude Interface Oscillations.)

research group tested at low enough steam flux to reach the relatively stationary interface regime. This map is useful even for waterhammer situations as it has been shown by Rothe *et al.* (1977a, 1978a) that $R_T > 1$ is a necessary condition for waterhammer.

The qualitative features of figures 19 and 20 are also useful for softer steam supplies. Although it is hard to define a liquid flux for steam injection into a pool as mapped in figure 9, all four regimes of figures 19 and 20 can be seen. When the pool subcooling is sufficient so that the effective thermodynamic ratio is large, moving horizontally across figure 9 corresponds to moving upward in the $R_T > 1$ region of figures 19 and 20; as the steam flux is increased one moves from a stationary interface regime, through a region of large interface oscillations, to a region where condensation takes place at the rapidly fluctuating surface of a jet or "flame". When the liquid pool does not have sufficient volume or subcooling, some steam escapes uncondensed as it does in the interface excursion region ($R_T < 1$) of figures 19 and 20.

It is expected that the reader has other examples to map onto figure 19.

This paper has shown several situations where an instability mechanism has triggered rapid condensation. The basic physics of this process remain to be examined in detail. Nevertheless, many situations where rapid condensation is triggered can be readily modeled and analyzed without the need to understand the details of the condensation processes.

Acknowledgements—Work that has led to this paper has been supported by EPRI, NRC, GE, CE, ASEA-ATOM, Creare Inc., and various electric utilities, and this support is gratefully acknowledged. The author also thanks Paul Rothe, Margaret Ackerson, Sherry Rhodes and Dodd Stacy for their assistance in preparing this paper.

REFERENCES

BANKOFF, S. G. TANKIN, R. S. & YUEN, M. C. 1978 Steam water mixing studies. Presented at the 6th Water Reactor Safety Res. Infor. Meeting, November.

BANKOFF, S. G., TANKIN, R. S. & YUEN, M. C. 1979 Condensation rates in steam/water mixing. Annual Progress Report to NRC, January.

BATCHELOR, D., CECCHI, T. & SHAH, V. 1976 Analysis of Tihange main feedwater lines behavior during a waterhammer event. *6th FORATOM Cong.*, Madrid.

BATT, D. L. 1978 Quick look report on LOFT nuclear experiment L2-2. LOFT TR-103, figure 33, December.

BIASI, J., PROSPERETTI, A. & TOZZI, A. 1972 Collapse of a condensing bubble in compressible liquids. *Chem. Engng Sci.* **27**, 815–822.

BLOCK, J. A. & CROWLEY, C. J. 1976 Lower plenum voiding, periodic delivery behavior, and transient tests at 1/15-scale. Creare Rep. TN-247, October.

BLOCK, J. A. & SCHROCK, V. E. 1977 Emergency cooling water delivery to the core inlet of PWRs during LOCA. *Symp. on the Thermal and Hydraulic Aspects of Nuclear Reactor Safety*, Vol. 1, *Light Water Reactors*, pp. 109–132. ASME-WAM, New York.

BLOCK, J. A., ROTHE, P. H., FANNING, M. W., CROWLEY, C. J. & WALLIS, G. B. 1976 Analysis of ECC delivery. Creare Rep. TN-231, April.

BOARD, S. J. & KIMPTON, A. D. 1974 Spherical vapour bubble collapse. *Chem. Engng Sci.* **29**, 363–371.

BRENNEN, C. 1978 Private communication.

CHAN, C. K., DHIR, V. K. & LIU, C. Y. 1978 Studies of dynamic loads in pressure suppression containment. Presentation at the 6th Water Reactor Safety Res. Info. Meeting, November.

CRAPO, H. S., JENSEN, M. F., SACKETT, K. E. & ZENDER, S. N. 1975 Experiment data report for semiscale MOD-1 test S-01-1B. Aerojet Nuclear Company Rep. ANCR-1199, May.

CROWLEY, C. J., WALLIS, G. B. & ROTHE, P. H. 1977 Preliminary analysis of condensation-induced transients. Creare Rep. TN-271, November.

FLORSCHUETZ, L. W. & CHAO, B. T. 1965 On the mechanics of vapor bubble collapse. *J. Heat Transfer, Trans. ASME* **87**, 209–220.

HAWTIN, P., HENWOOD, G. A. & HUBER, R. A. 1970 On the collapse of water vaprus cavities in a bubble analogue apparatus. *Chem. Engng Sci.* **25**, 1197–1209.

HICKLING, R. & PLESSET, M. S. 1964 Collapse and rebound of a spherical bubble in water. *Physics of Fluids* 7(1), 7–14.

KOSKY, P. G. & HENWOOD, G. A. 1969 A new technique for investigating vapour bubble implosion experimentally. Br. J. Appl. Phys. 2, 630–634.

LI, W. H. 1962 Mechanics of pipe flow following column separation. *J. Engng Mech. DIV. ASCF* 97–118, August.

MAA, J. R. 1969 Condensation of vapor on a very cold liquid stream. *I & EC Fundament.* **8**(3), 560–563.

ROTHE, P. H. & BLOCK, J. A. 1977 Aerodynanic behavior of liquid sprays. *Int. J. Multiphase Flow* 3, 263–272.

ROTHE, P. H., BLOCK, J. A. & WALLIS, G. B. 1976 An evaluation of the possibility of cold leg ECC flow oscillations in PWRs. Creare Rep. TN-240, June.

BLOCK, J. A., ROTHE, P. H., CROWLEY, C. J., WALLIS, G. B. & YOUNG, L. R. 1977a An evaluation of PWR steam generator waterhammer. Creare Rep. TN-251 (NUREG-0291), June.

ROTHE, P. H., WALLIS, G. B. & BLOCK, J. A. 1977b Cold leg ECC flow oscillations. *Symp. on the Thermal and Hydraulic Aspects of Nuclear Reactor Safety*, Vol. 1, *Light Water Reactor*, pp. 133–150. ASME-WAM, New York.

ROTHE, P. H., WALLIS, G. B. & CROWLEY, C. J. 1978a Waterhammer in the feedwater systems of PWR steam generators. In *Fluid Transients and Acoustics in the Power Industry*. ASME-WAM, New York.

ROTHE, P. H., WALLIS, G. B., FANNING, M. & BLOCK, J. A. 1978b A preliminary study of annulus ECC flow oscillations. Creare Rep. TM-517 (EPRI NP-839), August.

ROTHE, P. H. & CROWLEY, C. J. 1978 Scaling of pressure and subcooling for countercurrent flow. Creare Rep. TN-285 (NUREG/CR-0464), October.

SARGIS, D. A., STUHMILLER, J. H. & WANG, S. S. 1978 A fundamental thermalhydraulic model to predict steam chugging phenomena. In *Topics in Two-Phase Heat Transfer and Flow*, pp. 123–133. ASME-WAM, New York.

STANFORD, L. E. & WEBSTER, C. C. 1972 Energy suppression and fission product transport in pressure-suppression pools. Oak Ridge National Laboratory Rep. 3448, April.

SURSOCK, J. P. & DUFFEY, R. B. 1978 Condensation of steam bubbles in a subcooled pool. In *Topics in Two-Phase Heat Transfer and Flow*, pp. 135–141. ASME-WAM, New York.

TEOFANOUS, T. G., BIASI, L., ISBIN, H. S. & FAUSKE, H. K. 1969 Nonequilibrium bubble collapse: A theoretical study. *Chem. Engng, Prog. Symp. Series* **66**, 37–47.

WESTENDORF, W. H. & BROWN, W. F. 1966 Stability of intermixing of high-velocity vapor with its subcooled liquid in concurrent systems. NASA-TN-D-3553, October.